

# Fast spin $\pm 2$ spherical harmonics transforms and application in cosmology

Y. Wiaux

*Signal Processing Institute, Ecole Polytechnique Fédérale de Lausanne (EPFL),  
CH-1015 Lausanne, Switzerland*

L. Jacques

*Communications and Remote Sensing Laboratory, Université catholique de  
Louvain (UCL), B-1348 Louvain-la-Neuve, Belgium*

P. Vandergheynst

*Signal Processing Institute, Ecole Polytechnique Fédérale de Lausanne (EPFL),  
CH-1015 Lausanne, Switzerland*

---

## Abstract

An exact fast algorithm is developed for the spin-weighted spherical harmonics transforms of band-limited spin  $\pm 2$  functions on the sphere. First, we recall the notion of spin functions on the sphere and their decomposition in an orthonormal basis of spin-weighted spherical harmonics. Second, we discuss the *a priori*  $\mathcal{O}(L^4)$  asymptotic complexity of the spin  $\pm 2$  spherical harmonics transforms, where  $2L$  stands for the square-root of the number of sampling points on the sphere, also setting a band limit  $L$  for the spin  $\pm 2$  functions considered. We derive an explicit expression for the spin  $\pm 2$  spherical harmonics  $_{\pm 2}Y_{lm}$  (of integer  $l$  and  $m$ , with  $l \geq 2$ ,  $|m| \leq l$ ) as linear combinations of the standard scalar spherical harmonics  $Y_{lm}$  and  $Y_{(l-1)m}$ . An exact algorithm is developed for the spin  $\pm 2$  spherical harmonics transforms on equi-angular grids, based on the Driscoll and Healy fast scalar spherical harmonics transform. The theoretical exactness of the transform relies on a sampling theorem existing on equi-angular grids. The associated asymptotic complexity is of order  $\mathcal{O}(L^2 \log^2 L)$ . Alternative algorithms exist on other pixelizations, based on the technique of separation of variables. However, they are not theoretically exact and have an associated asymptotic complexity of order  $\mathcal{O}(L^3)$ . Finally, we consider the application of these generic developments in cosmology, for the efficient computation of the cosmic microwave background (CMB) invariant angular power spectra from the observable temperature  $T$  and the linear polarization Stokes parameters  $Q$  and  $U$  (direct transform), or for the simulation of temperature and polarization maps from theoretical spectra (inverse transform).

*Key words:* computational methods, data analysis, cosmology, cosmic microwave background.

---

## 1 Introduction

In the last few years, the analysis of the temperature anisotropies of the cosmic microwave background (CMB), together with other cosmological observations, has allowed the definition of a precise concordance cosmological model. These observations culminated with the release of the data of the Wilkinson Microwave Anisotropy Probe (WMAP) satellite mission. The cosmological parameters are now determined with an unprecedented precision of the order of several percent [1,2,3]. In the concordance model, the CMB originates from quantum energy fluctuations defined in a primordial era of inflation. These tiny fluctuations are Gaussian in first approximation. The cosmological principle of homogeneity and isotropy of the universe is also assumed. The observed radiation is therefore understood as a unique realization of a Gaussian and stationary (*i.e.* homogeneous and isotropic) random process on the sphere, which may be completely characterized from its two-points correlation functions, or the corresponding angular power spectra.

The present concordance values of the cosmological parameters are obtained through a best fit of the theoretical temperature angular power spectrum of the CMB with the experimental data. Beyond temperature or intensity anisotropies, a polarization of the CMB is also present and constitutes a complementary source of information for cosmology. This polarization is produced through Thomson scattering at the epoch of recombination. The degree of polarization of the CMB is expected to be of the order of 10 percent of the temperature anisotropies at small scales, and lower at large scales. As Thomson scattering only produces linearly polarized light, the CMB radiation is completely described by its temperature  $T$ , and its linear polarization Stokes parameters  $Q$  and  $U$  [4,5,6,7,8,9]. First polarization measurements have been reported only recently. Future CMB experiments such as the Planck surveyor satellite mission will allow a deeper probe of the temperature and polarization spectra, thanks to improved sensitivity and resolution on the whole sky.

From the mathematical point of view, the observable temperature  $T$  is a scalar function on the sphere, *i.e.* invariant under local rotations in the plane tangent to the sphere at each point. The associated invariant  $TT$  angular power spectrum results from the decomposition of the temperature in scalar spher-

---

*Email address:* `yves.wiaux@epfl.ch` (Y. Wiaux).

ical harmonics. But the observable polarization Stokes parameters  $Q$  and  $U$  transform as the components of a transverse, symmetric, and traceless rank 2 tensor under local rotations. However, scalar electric  $E$  and magnetic  $B$  polarization components may equivalently be defined from the parameters  $Q$  and  $U$ . The associated invariant  $EE$  and  $BB$  polarization angular power spectra, and the cross-correlation  $TE$  spectrum result from the decomposition of the combinations  $Q \pm iU$  in spin  $\pm 2$  spherical harmonics on the sphere [5], rather than in standard scalar spherical harmonics. From the numerical point of view, the asymptotic complexity associated with a naive quadrature based on the definition of the scalar and spin  $\pm 2$  spherical harmonics transforms is of order  $\mathcal{O}(L^4)$ , where  $L$  roughly identifies the square-root of the number of sampling points on the sphere. Corresponding computation times for the analysis of megapixels all-sky maps such as those of the ongoing WMAP or the forthcoming Planck missions are of the order of days. Fast and precise calculation methods for the scalar and spin  $\pm 2$  spherical harmonics transforms of functions on the sphere are therefore needed. Algorithms have already been defined which are widely used in the context of astrophysics and cosmology. We quote the HEALPix package defined on a Hierarchical Equal Area iso-Latitude Pixelization of the sphere [10,11], or the GLESP package defined on a Gauss-Legendre Sky Pixelization [12,13]. Those algorithms provide an asymptotic complexity of order  $\mathcal{O}(L^3)$ , which is not yet optimal. Moreover, they are not theoretically exact.

In the present work we develop a fast algorithm for the spin  $\pm 2$  spherical harmonics transforms of band-limited functions on the sphere, based on an existing exact fast algorithm for the scalar spherical harmonics transform. It is defined on  $2L \times 2L$  equi-angular pixelizations in spherical coordinates  $(\theta, \varphi)$  on the sphere. The algorithm is theoretically exact thanks to the existence of a sampling theorem on equi-angular grids. The associated optimized asymptotic complexity is of order  $\mathcal{O}(L^2 \log_2^2 L)$ . Corresponding computation times for megapixels maps are reduced to seconds. Beyond cosmology, the generic algorithm proposed here for the spin  $\pm 2$  spherical harmonics transforms will find application in the spectral analysis of arbitrary spin  $\pm 2$  signals on the sphere, components of transverse, symmetric, and traceless rank 2 tensor fields under local rotations. Notice that, depending on the application, each pixelization scheme (equi-angular, HEALPix, GLESP,...) may provide specific advantages. Notably, the fact of defining pixels of equal area represents an advantage of the HEALPix and GLESP pixelizations when dealing with noisy data. In that perspective, beyond its quoted advantages relative to previously defined algorithms, our algorithm may also be understood as a simple alternative defined on another pixelization of the sphere. The detailed comparison of the alternative algorithms and their relative advantages beyond theoretical exactness and asymptotic complexity is out of the scope of the present work.

In § 2, we discuss the standard harmonic analysis on the sphere and on the

rotation group  $SO(3)$ . We also recall the notion of spin  $n$  functions on the sphere and their harmonic decomposition in terms of spin-weighted spherical harmonics of spin  $n$ . In § 3, we first define equi-angular pixelizations and quote their major properties. Notably, we recall a sampling theorem on the sphere for band-limited functions with band limit  $L$  on  $2L \times 2L$  equi-angular pixelizations. We then discuss the *a priori*  $\mathcal{O}(L^4)$  asymptotic complexity for the scalar and spin  $\pm 2$  spherical harmonics transforms from their definitions and motivate the need for fast algorithms in the perspective of the CMB analysis. We also discuss the technique of separation of variables which is already used in existing fast algorithms and which provides an  $\mathcal{O}(L^3)$  asymptotic complexity. We finally develop an exact fast algorithm with complexity  $\mathcal{O}(L^2 \log^2 L)$  for the spin  $\pm 2$  spherical harmonics transforms on equi-angular grids. We also analyze our corresponding numerical implementation in terms of computation times, memory requirements, and numerical stability. In § 4, we recall the notion of the Stokes parameters associated with the polarized radiation of the CMB on the celestial sphere. We identify the corresponding invariant temperature and polarization angular power spectra. We illustrate the interest of our implementation both for the estimation of those spectra from the observable  $T$ ,  $Q$ , and  $U$  maps (direct transform), and for the simulation of temperature and polarization maps from theoretical spectra (inverse transform). We finally briefly conclude in § 5.

## 2 Spin $n$ functions on the sphere

In this section, we first reintroduce the standard scalar spherical harmonics and the Wigner  $D$ -functions as orthogonal basis functions for the decomposition of square-integrable functions on the sphere and on the rotation group  $SO(3)$  respectively. Second, we discuss the notion of spin  $n$  square-integrable functions on the sphere and their decomposition in a basis of spin-weighted spherical harmonics of spin  $n$ . The relation between the spin-weighted spherical harmonics of spin  $n$  and scalar spherical harmonics is also studied, through the action of the so-called spin raising and lowering operators.

### 2.1 Standard harmonic analysis on $S^2$ and $SO(3)$

Let the function  $G(\omega)$  be a square-integrable function in  $L^2(S^2, d\Omega)$  on the unit sphere  $S^2$ . The spherical coordinates of a point on the sphere, defined in the right-handed Cartesian coordinate system  $(o, o\hat{x}, o\hat{y}, o\hat{z})$  centered on the unit sphere, read as  $\omega = (\theta, \varphi)$ . The angle  $\theta \in [0, \pi]$  is the polar angle, or co-latitude. The angle  $\varphi \in [0, 2\pi[$  is the azimuthal angle, or longitude. The invariant measure on the sphere reads  $d\Omega = d\cos\theta d\varphi$ . The standard

scalar spherical harmonics  $Y_{lm}(\omega)$ , with  $l \in \mathbb{N}$ ,  $m \in \mathbb{Z}$ , and  $|m| \leq l$ , form an orthonormal basis for the decomposition of functions in  $L^2(S^2, d\Omega)$  on the sphere [14]. They are explicitly given in a factorized form in terms of the associated Legendre polynomials  $P_l^m(\cos \theta)$  and the complex exponentials  $e^{im\varphi}$  as

$$Y_{lm}(\theta, \varphi) = \left[ \frac{2l+1}{4\pi} \frac{(l-m)!}{(l+m)!} \right]^{1/2} P_l^m(\cos \theta) e^{im\varphi}. \quad (1)$$

This corresponds to the choice of Condon-Shortley phase  $(-1)^m$  for the spherical harmonics, insuring the relation  $(-1)^m Y_{lm}^*(\omega) = Y_{l(-m)}(\omega)$ . This phase is here included in the definition of the associated Legendre polynomials [15,14]. Another convention [16] explicitly transfers it to the spherical harmonics. The orthonormality and completeness relations respectively read:

$$\int_{S^2} d\Omega Y_{lm}^*(\omega) Y_{l'm'}(\omega) = \delta_{ll'} \delta_{mm'}, \quad (2)$$

and

$$\sum_{l \in \mathbb{N}} \sum_{|m| \leq l} Y_{lm}^*(\omega') Y_{lm}(\omega) = \delta(\omega' - \omega), \quad (3)$$

with  $\delta(\omega' - \omega) = \delta(\cos \theta' - \cos \theta) \delta(\varphi' - \varphi)$ . Any function  $G(\omega)$  on the sphere is thus uniquely given as a linear combination of scalar spherical harmonics (inverse transform):

$$G(\omega) = \sum_{l \in \mathbb{N}} \sum_{|m| \leq l} \hat{G}_{lm} Y_{lm}(\omega), \quad (4)$$

for the scalar spherical harmonics coefficients (direct transform)

$$\hat{G}_{lm} = \int_{S^2} d\Omega Y_{lm}^*(\omega) G(\omega), \quad (5)$$

with  $|m| \leq l$ .

Let now  $G(\rho)$  be a square-integrable function in  $L^2(SO(3), d\rho)$  on the group  $SO(3)$  of three-dimensional rotations. Any rotation  $\rho \in SO(3)$  may be explicitly given in the Euler angles parametrization as  $\rho = (\varphi, \theta, \chi)$ , describing successive rotations by the Euler angles  $\chi \in [0, 2\pi[$ ,  $\theta \in [0, \pi]$ , and  $\varphi \in [0, 2\pi[$ , around the axes of coordinate  $o\hat{z}$ ,  $o\hat{y}$ , and  $o\hat{z}$  respectively. The invariant measure on the rotation group reads  $d\rho = d\varphi d\theta d\chi$ . The Wigner  $D$ -functions  $D_{mn}^l(\rho)$ , with  $l \in \mathbb{N}$ ,  $m, n \in \mathbb{Z}$ , and  $|m|, |n| \leq l$ , are the matrix elements of the irreducible unitary representations of weight  $l$  of the rotation group  $SO(3)$ , in  $L^2(SO(3), d\rho)$ . By the Peter-Weyl theorem on compact groups, the matrix elements  $D_{mn}^{l*}$  also form an orthogonal basis in  $L^2(SO(3), d\rho)$  [14]. They are explicitly given in a factorized form in terms of the real Wigner  $d$ -functions  $d_{mn}^l(\theta)$  and the complex exponentials  $e^{-im\varphi}$  and  $e^{-in\chi}$  as

$$D_{mn}^l(\varphi, \theta, \chi) = e^{-im\varphi} d_{mn}^l(\theta) e^{-in\chi}. \quad (6)$$

The Wigner  $d$ -functions read

$$d_{mn}^l(\theta) = \sum_{t=C_1}^{C_2} \frac{(-1)^t [(l+m)!(l-m)!(l+n)!(l-n)!]^{1/2}}{(l+m-t)!(l-n-t)!t!(t+n-m)!} (\cos \theta/2)^{2l+m-n-2t} (\sin \theta/2)^{2t+n-m}, \quad (7)$$

with the summation bounds  $C_1 = \max(0, m-n)$  and  $C_2 = \min(l+m, l-n)$  defined to consider only factorials of positive integers. They satisfy various symmetry properties on their indices [14]. The orthogonality and completeness relations of the Wigner  $D$ -functions respectively read:

$$\int_{SO(3)} d\rho D_{mn}^l(\rho) D_{m'n'}^{l'*}(\rho) = \frac{8\pi^2}{2l+1} \delta_{ll'} \delta_{mm'} \delta_{nn'}, \quad (8)$$

and

$$\sum_{l \in \mathbb{N}} \frac{2l+1}{8\pi^2} \sum_{|m|, |n| \leq l} D_{mn}^l(\rho') D_{mn}^{l'*}(\rho) = \delta(\rho' - \rho), \quad (9)$$

with  $\delta(\rho' - \rho) = \delta(\varphi' - \varphi) \delta(\cos \theta' - \cos \theta) \delta(\chi' - \chi)$ . Any function  $G(\rho)$  in  $L^2(SO(3), d\rho)$  is thus uniquely given as a linear combination of Wigner  $D$ -functions (inverse transform):

$$G(\rho) = \sum_{l \in \mathbb{N}} \frac{2l+1}{8\pi^2} \sum_{|m|, |n| \leq l} \hat{G}_{mn}^l D_{mn}^{l'*}(\rho), \quad (10)$$

for the Wigner  $D$ -functions coefficients (direct transform)

$$\hat{G}_{mn}^l = \int_{SO(3)} d\rho D_{mn}^l(\rho) G(\rho), \quad (11)$$

with  $|m|, |n| \leq l$ .

## 2.2 Spin $n$ functions on the sphere

Let us define a spin  $n$  square-integrable function  ${}_nG(\omega)$  in  $L^2(S^2, d\Omega)$  on the sphere. As already discussed, in the coordinate system  $(o, o\hat{x}, o\hat{y}, o\hat{z})$ , the Euler angles  $(\varphi, \theta, \chi)$  associated with a general rotation  $\rho$  in three dimensions represent successive rotations by  $\chi$  around  $o\hat{z}$ ,  $\theta$  around  $o\hat{y}$ , and  $\varphi$  around  $o\hat{z}$ . These may also be interpreted in the reverse order as successive rotations by  $\varphi$  around  $o\hat{z}$ ,  $\theta$  around  $o\hat{y}'$ , and  $\chi$  around  $o\hat{z}''$ , where the axes  $o\hat{y}' \equiv o\hat{y}'(\varphi)$  and  $o\hat{z}'' \equiv o\hat{z}''(\varphi, \theta)$  are respectively obtained by the first and second rotations of the coordinate system by  $\varphi$  and  $\theta$  [16]. The local rotations of the basis vectors in the plane tangent to the sphere at  $\omega = (\theta, \varphi)$  are rotations around  $o\hat{z}''$ , therefore associated with the third Euler angle  $\chi$ . Spin  $n$  functions on the

sphere  ${}_nG(\omega)$ , with  $n \in \mathbb{Z}$ , are defined relatively to their behaviour under the corresponding right-handed rotations by  $\chi_0$  as [17,18,19]:

$${}_nG'(\omega) = e^{-in\chi_0} {}_nG(\omega). \quad (12)$$

The standard square-integrable functions on the sphere considered above are spin 0 or scalar functions. Let us emphasize that the rotations considered are local transformations on the sphere around the axis  $o\hat{z}'' \equiv o\hat{z}''(\varphi, \theta)$ , affecting the coordinate  $\chi$  in the tangent plane independently at each point  $\omega = (\theta, \varphi)$ , and according to  $\chi' = \chi - \chi_0$ . They are to be clearly distinguished from the global rotations by  $\chi$  around  $o\hat{z}$  associated with the alternative Euler angles interpretation, which affect the coordinates of the points  $\omega = (\theta, \varphi)$  on the sphere. Our sign convention in the exponential is coherent with the definition (13) below for the spin-weighted spherical harmonics of spin  $n$ . It is opposite to the original definition [17], while equivalent to recent notations used in the context of the CMB analysis [5,9].

Recalling the factorized form (6), spin functions are equivalently defined as the evaluation at  $\chi = 0$  of any function in  $L^2(SO(3), d\rho)$  resulting from an expansion for fixed index  $n$  in the Wigner  $D$ -functions  $D_{mn}^l(\varphi, \theta, \chi)$ . The functions  $D_{mn}^l(\varphi, \theta, 0)$  or  $D_{m(-n)}^{l*}(\varphi, \theta, 0)$  thus naturally define for each  $n$  an orthogonal basis for the expansion of spin  $n$  functions in  $L^2(S^2, d\Omega)$  on the sphere. Their normalization in  $L^2(S^2, d\Omega)$  defines the spin-weighted spherical harmonics of spin  $n$ :

$${}_nY_{lm}(\theta, \varphi) = (-1)^n \sqrt{\frac{2l+1}{4\pi}} D_{m(-n)}^{l*}(\varphi, \theta, 0), \quad (13)$$

with  $l \in \mathbb{N}$ ,  $l \geq |n|$ , and  $m \in \mathbb{Z}$ ,  $|m| \leq l$ . They are thus explicitly given in a factorized form in terms of the real Wigner  $d$ -functions  $d_{mn}^l(\theta)$  and the complex exponentials  $e^{im\varphi}$  as

$${}_nY_{lm}(\theta, \varphi) = (-1)^n \sqrt{\frac{2l+1}{4\pi}} d_{m(-n)}^l(\theta) e^{im\varphi}. \quad (14)$$

In particular, the symmetry properties of the Wigner  $d$ -functions imply the generalized symmetry relation  $(-1)^{n+m} {}_nY_{lm}^*(\omega) = -{}_nY_{l(-m)}(\omega)$ . The spin 0 spherical harmonics explicitly identify with the standard scalar spherical harmonics for the decomposition of scalar functions:  ${}_0Y_{lm}(\omega) = Y_{lm}(\omega)$ , through the relation  $d_{m0}^l(\theta) = \left[\frac{(l-m)!}{(l+m)!}\right]^{1/2} P_l^m(\cos \theta)$ . The orthonormality and completeness relations respectively read from relations (8) and (9), as

$$\int_{S^2} d\Omega {}_nY_{lm}^*(\omega) {}_nY_{l'm'}(\omega) = \delta_{ll'} \delta_{mm'}, \quad (15)$$

and

$$\sum_{l \in \mathbb{N}} \sum_{|m| \leq l} {}_nY_{lm}^*(\omega') {}_nY_{lm}(\omega) = \delta(\omega' - \omega), \quad (16)$$

with  $\delta(\omega' - \omega) = \delta(\cos \theta' - \cos \theta) \delta(\varphi' - \varphi)$ . Any spin  $n$  function  ${}_nG(\omega)$  on the sphere is thus uniquely given as a linear combination of spin  $n$  spherical harmonics (inverse transform):

$${}_nG(\omega) = \sum_{l \in \mathbb{N}} \sum_{|m| \leq l} {}_n\hat{G}_{lm} {}_nY_{lm}(\omega), \quad (17)$$

for the spin-weighted spherical harmonics coefficients (direct transform)

$${}_n\hat{G}_{lm} = \int_{S^2} d\Omega {}_nY_{lm}^*(\omega) G(\omega), \quad (18)$$

with  $l \geq |n|$ , and  $|m| \leq l$ .

Finally, spin  $n \pm 1$  functions may be defined from spin  $n$  functions through the action of the so-called spin raising and lowering operators [17,18]. The action of the spin raising  $\bar{\partial}$  and lowering  $\partial$  operators on a spin  $n$  function  ${}_nG$ , giving spin  $n + 1$  and  $n - 1$  functions respectively, is defined as

$$[\partial {}_nG](\theta, \varphi) = \left[ -\sin^n \theta \left( \frac{\partial}{\partial \theta} + \frac{i}{\sin \theta} \frac{\partial}{\partial \varphi} \right) \sin^{-n} \theta {}_nG \right](\theta, \varphi), \quad (19)$$

and

$$[\bar{\partial} {}_nG](\theta, \varphi) = \left[ -\sin^{-n} \theta \left( \frac{\partial}{\partial \theta} - \frac{i}{\sin \theta} \frac{\partial}{\partial \varphi} \right) \sin^n \theta {}_nG \right](\theta, \varphi), \quad (20)$$

with, under rotation by  $\chi_0$  in the tangent plane at  $\omega = (\theta, \varphi)$ :  $[\partial {}_nG]'(\omega) = e^{-i(n+1)\chi_0} [\partial {}_nG](\omega)$  and  $[\bar{\partial} {}_nG]'(\omega) = e^{-i(n-1)\chi_0} [\bar{\partial} {}_nG](\omega)$ . In these terms, the spin-weighted spherical harmonics of spin  $n$  are related to spin-weighted spherical harmonics of spins  $n + 1$  and  $n - 1$  through the following relations:

$$[\partial {}_nY_{lm}](\omega) = [(l - n)(l + n + 1)]^{1/2} {}_{n+1}Y_{lm}(\omega), \quad (21)$$

and

$$[\bar{\partial} {}_nY_{lm}](\omega) = -[(l + n)(l - n + 1)]^{1/2} {}_{n-1}Y_{lm}(\omega), \quad (22)$$

also implying

$$[\bar{\partial} \partial {}_nY_{lm}](\omega) = -(l - n)(l + n + 1) {}_nY_{lm}(\omega). \quad (23)$$

The corresponding direct relation between the spin-weighted spherical harmonics of spin  $n$  and scalar spherical harmonics reads:

$${}_nY_{lm}(\omega) = \left[ \frac{(l - n)!}{(l + n)!} \right]^{1/2} [\partial^n Y_{lm}](\omega), \quad (24)$$

for  $0 \leq n \leq l$ , and

$${}_nY_{lm}(\omega) = \left[ \frac{(l + n)!}{(l - n)!} \right]^{1/2} (-1)^n [\bar{\partial}^{-n} Y_{lm}](\omega), \quad (25)$$



for  $-l \leq n \leq 0$ .

These relations between spin-weighted and scalar spherical harmonics are explicitly used in § 3 for the development of a fast direct spin  $\pm 2$  spherical harmonics transforms algorithm.

### 3 Fast spin $\pm 2$ transforms algorithm

In this section, we first define equi-angular pixelizations on the sphere and discuss their major properties, notably the fact that they imply the existence of a sampling theorem. Second, we calculate the *a priori*  $\mathcal{O}(L^4)$  asymptotic complexity associated with the computation of scalar and spin  $\pm 2$  spherical harmonics transforms from their definitions. In the perspective of the CMB temperature and polarization analysis, this motivates the development of fast algorithms. Third, we develop an exact fast algorithm for the calculation of the spin  $\pm 2$  spherical harmonics transforms of band-limited functions on equi-angular grids on the sphere. The algorithm is based on an expression of the spin-weighted spherical harmonics of spin  $\pm 2$  as simple linear combinations without derivatives of scalar spherical harmonics, and on the already existing Driscoll and Healy fast scalar spherical harmonics transform. The exactness of the computation relies on the sampling theorem established for equi-angular pixelizations. The related asymptotic complexity is of order  $\mathcal{O}(L^2 \log_2^2 L)$  for band-limited functions with band limit  $L$ . The algorithm advantageously compares with alternative approximate  $\mathcal{O}(L^3)$  algorithms based on the technique of separation of variables. Finally, we produce the numerical implementation of our algorithm and analyze the computation times, the memory requirements, and the numerical stability for fine samplings on the sphere, with band limits up to  $L = 1024$ .

#### 3.1 Equi-angular sampling



Figure 1. Equi-angular grids at resolutions  $L = 4$  (left) and  $L = 8$  (right).

A  $2L \times 2L$  equi-angular grid in spherical coordinates  $(\theta, \varphi)$  is defined on points  $\omega_{ij} = (\theta_i, \varphi_j)$  for  $0 \leq i, j \leq 2L - 1$ , with a uniform discretization of the coordinates:  $\Delta\theta = \theta_{i+1} - \theta_i = \pi/2L$  and  $\Delta\varphi = \varphi_{j+1} - \varphi_j = 2\pi/2L$ . The specific choice  $\theta_0 = \pi/4L$ , and  $\varphi_0 = 0$  is considered in the following implementations. It gives  $\theta_i = (2i + 1)\pi/4L$  and  $\varphi_j = 2j\pi/2L$ , and excludes the poles of the sampling, which can be convenient for numerical reasons. The figure 1 illustrates the equi-angular sampling for resolutions  $L = 4$  and  $L = 8$ . The pixels centers are identified with the sampling points  $\omega_{ij}$  defined here above. The pixels edges are identified by meridians shifted by  $\Delta\theta/2 = \pi/4L$ , and parallels shifted by  $\Delta\varphi/2 = 2\pi/4L$  relative to  $\omega_{ij}$ . The poles therefore appear as pixels corners. In the following, we emphasize various important properties of the equi-angular sampling.

First, as will be emphasized in subsection 3.3, the fast computation of scalar or spin  $\pm 2$  spherical harmonics transforms notably relies on the fact that the sampling in the polar angle  $\theta$  is independent of the azimuthal angle  $\varphi$ . This property defines so-called iso-latitude pixelizations. Many pixelization schemes have been considered on the sphere which satisfy this requirement. It is the case for the equi-angular pixelization, as well as for standard grids in astrophysics such as the HEALPix pixelization (Hierarchical Equal Area iso-Latitude Pixelization) [10,11], and the GLESP pixelization (Gauss-Legendre Sky Pixelization) [12,13].

Second, the area of pixels,  $A(\omega_{ij}) \simeq \sin\theta_i \Delta\theta \Delta\varphi$ , varies considerably with the co-latitude, from small pixels close to the poles, to larger pixels around the equator (see figure 1). This is a major difference with the HEALPix pixelization which defines equal-area pixels, or the GLESP pixelization which defines nearly equal-area pixels. The constant area of pixels is a property of interest in the treatment of noisy data [10]. Also notice, that equal-area pixels is an important property allowing the definition of a pixel window function associated to a given pixelization at a given resolution. The main interest of this concept is to apply a low-pass filtering to the signal, implementing the fact that the pixelized signal is smoothed by integration over the pixel area. The corresponding window function depends on the pixelization structure and resolution. The procedure of pixelization is approximated to a correlation of the signal with an axisymmetric beam, and therefore strongly relies on the assumption of equal-area pixels. We do not consider here the generalization of this concept on equi-angular pixelizations, where the pixel area varies drastically over the surface of the sphere. This problematic lies beyond the scope of the present article. We simply restrict ourselves to the analysis of band-limited signals, in which case variations of the signal over the pixel area can be neglected, and the use of the pixel window function can be avoided. In that respect, in order to achieve the limit frequency  $L$ , the naive extrapolation of the Nyquist-Shannon theorem on the line typically requires  $2L$  sampling points in the angles  $\theta$  and  $\varphi$  on the sphere, *i.e.* pixelizations on  $N_p = (2L)^2$

points, independently of the pixelization structure.

Finally, an exact sampling theorem exists on equi-angular pixelizations on the sphere, generalization of the Nyquist-Shannon theorem on the line. Let us consider band-limited functions  $G(\omega)$  on the sphere with band limit  $L$ , defined through the following condition on their scalar spherical harmonics coefficients:  $\hat{G}_{lm} = 0$  for  $l \geq L$ . Equivalently, a function  $G(\rho)$  on  $SO(3)$  has a band limit  $L$  if and only if  $\hat{G}_{mn}^l = 0$  for  $l \geq L$ . The sampling theorem states that the scalar spherical harmonics coefficients of a band-limited function on the sphere may be computed exactly up to a band limit  $L$ , through a  $2L \times 2L$  equi-angular sampling, as a finite weighted sum, *i.e.* a quadrature, of the sampled values of that function [20]. The weights are defined from the structure of the Legendre polynomials  $P_l(\cos \theta)$  on the interval  $[0, \pi]$ . This result is also valid on  $SO(3)$  through a  $2L \times 2L \times 2L$  equi-angular sampling in  $\rho = (\varphi, \theta, \chi)$  [21,22]. A spin  $n$  function  ${}_nG$  on the sphere is band-limited at some band limit  $L$  if and only if the following condition holds on its spin-weighted spherical harmonics coefficients:  ${}_n\hat{G}_{lm} = 0$  for  $l \geq L$ . The sampling theorem on  $SO(3)$  may be easily restricted to spin  $n$  functions on the sphere, thus generalizing the sampling theorem on the sphere to the decomposition of either scalar or spin  $n$  functions.

This sampling theorem is only established for equi-angular grids. It therefore represents a major advantage of equi-angular pixelizations relative to HEALPix and GLESP pixelizations. For the sake of the theoretical exactness of the direct scalar and spin-weighted spherical harmonics transforms algorithms,  $2L \times 2L$  equi-angular grids on the sphere are consequently considered in the following. Notice in that respect that, the exactness of a spin  $\pm 2$  spherical harmonics transforms algorithm based on a simple separation of variables would explicitly require the sampling theorem for spin  $n$  functions on the sphere. However, as our algorithm defined below computes spin  $\pm 2$  spherical harmonics transforms at the band limit  $L$  in terms of scalar spherical harmonics transforms at the same band limit, it will only require the sampling theorem established for scalar functions on  $2L \times 2L$  equi-angular grids.

### 3.2 *A priori $\mathcal{O}(L^4)$ complexity and separation of variables*

As discussed in detail in § 4, the estimation of the CMB angular power spectra from experimental all-sky maps requires the computation of the direct scalar and spin  $\pm 2$  spherical harmonics transforms of the temperature ( $T$ ) and polarization ( $Q \pm iU$ ) maps respectively. Corresponding inverse transforms are required to simulate maps from theoretical spectra. Consequently, the fast and precise computation of (direct and inverse) scalar and spin  $\pm 2$  spherical harmonics transforms of functions on the sphere is fundamental in that respect. For a signal with band-limit  $L$ , the *a priori* complexity associated with the

naive computation of the direct scalar spherical harmonics transform integral (5) on the sphere through simple discretization, *i.e.* a quadrature, for all  $(l, m)$  with  $|m| \leq l < L$ , is naturally of order  $\mathcal{O}(L^4)$ . And the *a priori* complexity associated with the naive computation of the direct spin  $\pm 2$  spherical harmonics transforms integrals (18) on the sphere through simple quadrature, for all  $(l, m)$  with  $l \geq 2$ , and  $|m| \leq l < L$ , is also naturally of order  $\mathcal{O}(L^4)$ . The same complexity naturally applies to the corresponding inverse scalar (4) or spin  $\pm 2$  (17) transforms. We consider fine samplings corresponding to megapixels maps on the sphere. In particular, the WMAP experiment currently provides all-sky maps of around three megapixels. For such a fine sampling defining a band limit around  $L \simeq 10^3$ , the typical computation time for  $(2L)^2$  multiplications and  $(2L)^2$  additions of double-precision numbers is of order of 0.03 seconds on a standard 2.2 GHz Intel Pentium Xeon CPU. We take this value as a fair estimation of the computation time required for one integration for given  $(l, m)$  in (5) or (18), or one summation for given  $(\theta, \varphi)$  in (4) or (17), with an associated  $\mathcal{O}(L^2)$  asymptotic complexity. Consequently, scalar or spin  $\pm 2$  spherical harmonics transforms, with an asymptotic complexity of order  $\mathcal{O}(L^4)$ , typically take several days at that band limit  $L \simeq 10^3$  on a single standard computer. Considering the analysis of a large number of signals or simulations may become difficultly affordable in terms of computation times.

The development of an exact fast algorithm is therefore of great interest for the CMB analysis, notably in the perspective of forthcoming experiments with improved resolution on the sky, such as the Planck satellite mission which will release all-sky maps of around fifty megapixels. The technique of separation of variables in the scalar (1) or spin  $\pm 2$  (14) spherical harmonics into the associated Legendre polynomials  $P_l^m(\cos \theta)$  or the Wigner  $d$ -functions  $d_{m2}^l(\theta)$ , and the complex exponentials  $e^{im\varphi}$  allows to decompose the transform as successive transforms in  $\varphi$  and  $\theta$  [23,21]. It naturally reduces the asymptotic complexity for the direct and inverse scalar and spin  $\pm 2$  spherical harmonics transforms to  $\mathcal{O}(L^3)$ . It can be implemented on any iso-latitude pixelization. The present algorithms used in the context of the CMB analysis, notably on HEALPix or GLESP pixelizations are indeed based on this technique. For the HEALPix pixelization, the present coding performances achieved already allow to reduce computation times for the transforms of megapixels maps from days to seconds. However, the  $\mathcal{O}(L^3)$  asymptotic complexity produced by the separation of variables is not yet optimal. Moreover, the HEALPix and GLESP implementations of the scalar and spin  $\pm 2$  spherical harmonics transforms are only approximate from the theoretical point of view as no sampling theorem is established on those pixelizations. The following subsection defines an exact algorithm on equi-angular grids, with an optimized  $\mathcal{O}(L^2 \log_2^2 L)$  asymptotic complexity.

### 3.3 New exact $\mathcal{O}(L^2 \log_2^2 L)$ algorithm on equi-angular pixelizations

We recall the following derivative relation on the associated Legendre polynomials [15],

$$\left[ \frac{\partial}{\partial \theta} P_l^m \right] (\cos \theta) = l \cot \theta P_l^m (\cos \theta) - \frac{l+m}{\sin \theta} P_{l-1}^m (\cos \theta), \quad (26)$$

under the convention that  $P_l^m$  is defined to be zero for  $l < |m|$ . Through this relation, the derivative relations (24) and (25) between the spin  $\pm 2$  spherical harmonics  ${}_{\pm 2}Y_{lm}$  and the scalar spherical harmonics  $Y_{lm}$  may be turned into a simple expression of  ${}_{\pm 2}Y_{lm}$  as linear combinations without derivatives of  $Y_{lm}$ ,  $Y_{(l-1)m}$ , and  $Y_{(l-2)m}$ . Notice that the same recurrence procedure is used in a different context in [24], in order to express spin  $n$  spherical harmonics  ${}_nY_{lm}$ , for any  $n$  with  $0 \leq |n| \leq l$ , as linear combinations of scalar spherical harmonics. Through the recurrence relation on  $l$  satisfied by the associated Legendre polynomials of given  $m$ ,

$$(l-m) P_l^m (\cos \theta) = (2l-1) \cos \theta P_{l-1}^m (\cos \theta) - (l+m-1) P_{l-2}^m (\cos \theta), \quad (27)$$

the  $Y_{(l-2)m}$  term in the quoted linear combination for  ${}_{\pm 2}Y_{lm}$  may be cancelled. We finally obtain the following expression of  ${}_{\pm 2}Y_{lm}$  as a linear combination of the scalar spherical harmonics  $Y_{lm}$  and  $Y_{(l-1)m}$ :

$${}_{\pm 2}Y_{lm} (\theta, \varphi) = \left[ \frac{(l-2)!}{(l+2)!} \right]^{1/2} \left[ \alpha_{(lm)}^{\pm} (\theta) Y_{lm} (\theta, \varphi) + \beta_{(lm)}^{\pm} (\theta) Y_{(l-1)m} (\theta, \varphi) \right], \quad (28)$$

for  $l \geq 2$  and  $|m| \leq l$ , and with the functional coefficients

$$\begin{aligned} \alpha_{(lm)}^{\pm} (\theta) &= \frac{2m^2 - l(l+1)}{\sin^2 \theta} \mp 2m(l-1) \frac{\cot \theta}{\sin \theta} + l(l-1) \cot^2 \theta \\ \beta_{(lm)}^{\pm} (\theta) &= 2 \left[ \frac{2l+1}{2l-1} (l^2 - m^2) \right]^{1/2} \left( \pm \frac{m}{\sin^2 \theta} + \frac{\cot \theta}{\sin \theta} \right). \end{aligned} \quad (29)$$

This relation holds once more under the convention that  $Y_{lm}$  is defined to be zero for  $l < |m|$ .

Consequently, the direct spin-weighted spherical harmonics transform of a spin  $\pm 2$  function  ${}_{\pm 2}G$  may be written as a linear combination of direct scalar spherical harmonics transforms for three associated scalar functions. Indeed, if the associated functions are defined by  $G^{(p)}(\theta, \varphi) = (\cot^p \theta / \sin^q \theta) {}_{\pm 2}G(\theta, \varphi)$ , for  $p, q \in \mathbb{N}$  and  $p+q=2$ , one gets from relation (28):

$$\begin{aligned}
{}_{\pm 2}\widehat{G}_{lm} = & \left[ \frac{(l-2)!}{(l+2)!} \right]^{1/2} \left\{ 2 \left[ \frac{2l+1}{2l-1} (l^2 - m^2) \right]^{1/2} \left( \widehat{G^{(1)}}_{(l-1)m} \pm m \widehat{G^{(0)}}_{(l-1)m} \right) \right. \\
& \left. + l(l-1) \widehat{G^{(2)}}_{lm} \mp 2m(l-1) \widehat{G^{(1)}}_{lm} + [2m^2 - l(l+1)] \widehat{G^{(0)}}_{lm} \right\},
\end{aligned} \tag{30}$$

with  $l \geq 2$  and  $|m| \leq l$ . The relation (3) also implies that the inverse spin-weighted transform of a set of spin  $\pm 2$  coefficients  ${}_{\pm 2}\widehat{G}_{lm}$  (with  ${}_{\pm 2}\widehat{G}_{lm} = 0$  for  $l \geq L$ ) may be written as a sum of three inverse scalar spherical harmonics transforms:

$$G(\theta, \varphi) = \frac{1}{\sin^2 \theta} A(\theta, \varphi) + \frac{\cot \theta}{\sin \theta} B(\theta, \varphi) + \cot^2 \theta C(\theta, \varphi), \tag{31}$$

with the scalar functions  $A$ ,  $B$ , and  $C$  identified as follows by their scalar spherical harmonics coefficients:

$$\begin{aligned}
\widehat{A}_{lm} = & \left[ \frac{(l-2)!}{(l+2)!} \right]^{1/2} [2m^2 - l(l+1)] {}_{\pm 2}\widehat{G}_{lm} \\
& \pm 2m \left[ \frac{(l-1)!(2l+3)}{(l+3)!(2l+1)} ((l+1)^2 - m^2) \right]^{1/2} {}_{\pm 2}\widehat{G}_{(l+1)m} \\
\widehat{B}_{lm} = & \left[ \frac{(l-2)!}{(l+2)!} \right]^{1/2} [\mp 2m(l-1)] {}_{\pm 2}\widehat{G}_{lm} \\
& + 2 \left[ \frac{(l-1)!(2l+3)}{(l+3)!(2l+1)} ((l+1)^2 - m^2) \right]^{1/2} {}_{\pm 2}\widehat{G}_{(l+1)m} \\
\widehat{C}_{lm} = & \left[ \frac{(l-2)!}{(l+2)!} \right]^{1/2} [l(l-1)] {}_{\pm 2}\widehat{G}_{lm}.
\end{aligned} \tag{32}$$

As discussed, for functions band-limited at  $L$ , the separation of variables allows to compute the direct and inverse scalar spherical harmonics transforms in  $\mathcal{O}(L^3)$  operations. However, an exact fast algorithm was developed by Driscoll and Healy on  $2L \times 2L$  equi-angular grids on the sphere for the scalar spherical harmonics transforms [20]. The Fourier transforms in  $e^{im\varphi}$  are computed in  $\mathcal{O}(L \log_2 L)$  operations for each  $\theta$  through standard Cooley-Tukey fast Fourier transforms. The algorithm also explicitly takes advantage of the recurrence relation in  $l$  on the associated Legendre polynomials  $P_l^m(\cos \theta)$  to compute the direct associated Legendre transforms in  $\mathcal{O}(L \log_2^2 L)$  operations for each  $m$ . In these terms, the direct and inverse scalar spherical harmonics transforms are computed in  $\mathcal{O}(L^2 \log_2^2 L)$  operations. The computation is theoretically exact. This fact relies, for the direct transform, on the specific choice of weighting functions only depending on  $\theta$ , as required by the sampling theorem on the sphere. Corresponding stable numerical implementations exist

in the SpharmonicKit package [25,26]<sup>1</sup>. Through the relations (30) and (31), the spin-weighted spherical harmonics transforms of a band-limited spin  $\pm 2$  function with band limit  $L$  may consequently also be computed exactly on a  $2L \times 2L$  equi-angular grid on the sphere from the Driscoll and Healy fast scalar spherical harmonics transforms. The exactness of the computation is obviously induced by the exactness of the Driscoll and Healy transforms. The number of operations required may be detailed as  $5 \times \mathcal{O}(L^2) + 3 \times \mathcal{O}(L^2 \log_2^2 L)$  for both the direct and inverse transforms. The corresponding asymptotic complexity is therefore  $\mathcal{O}(L^2 \log_2^2 L)$ , equivalent to the complexity associated with the scalar spherical harmonics transforms. In terms of our previous intuitive estimations, we recall that an  $\mathcal{O}(L^2)$  scalar product requires the order of 0.03 seconds on a standard 2.2 GHz Intel Pentium Xeon CPU, at band limits around  $L \simeq 10^3$ . When compared to the *a priori*  $\mathcal{O}(L^4)$  asymptotic complexity, the  $\mathcal{O}(L^2 \log_2^2 L)$  scalar and spin  $\pm 2$  spherical harmonics transforms algorithms consequently reduce computation times from days to seconds for the fine samplings considered.

Let us remark that a recurrence relation was proposed in [27] in order to compute spin  $n$  spherical harmonics transforms from scalar spherical harmonics transforms. However, the proposed relation explicitly relates  ${}_n Y_{lm}$  with  ${}_{n \mp 1} Y_{lm}$ ,  ${}_{n \mp 1} Y_{(l-1)m}$ , and  ${}_{n \mp 1} Y_{(l+1)m}$ . The term  ${}_{n \mp 1} Y_{(l+1)m}$  increases the band limit of the functions to be analyzed to  $L+2$  after the 2-steps recurrence leading from spin  $\pm 2$  to scalar spherical harmonics. On  $2L \times 2L$  equi-angular grids, the SpharmonicKit package is technically limited to consider coefficients lower than  $L$ , and numerical errors will occur due to the absence of consideration of the coefficients at  $l = L$  and  $l = L + 1$ . No such issue occurs from the relation (28) here above, which preserves the band limit  $L$  for the associated scalar functions.

### 3.4 Numerical implementation

We produced the numerical implementation of the  $\mathcal{O}(L^2 \log_2^2 L)$  spin-weighted spherical harmonics transforms for band-limited spin  $\pm 2$  functions with band limit  $L$  on  $2L \times 2L$  equi-angular grids on the sphere. As discussed, the implementation is directly based on the fast scalar spherical harmonics transform proposed by Driscoll and Healy and implemented in the SpharmonicKit package. We here report the corresponding computation times and memory requirements for band limits up to  $L = 1024$ , and briefly discuss the issue of the numerical stability of the implementation. Calculations are performed on a 2.20 GHz Intel Pentium Xeon CPU with 2 Gb of RAM memory. Random

---

<sup>1</sup> See [www.cs.dartmouth.edu/~geelong/sphere/](http://www.cs.dartmouth.edu/~geelong/sphere/) for unpublished documentation and algorithm implementation (SpharmonicKit package).

band-limited test-functions are considered. Without loss of generality, these test-functions are defined through their spin-weighted spherical harmonics coefficients  $_{\pm 2}\widehat{G}_{lm}$ , with  $|m| \leq l < L$ , and  $l \geq 2$ , with independent real and imaginary parts uniformly distributed in the interval  $[-1, +1]$ . The inverse and direct spin-weighted spherical harmonics transforms are successively computed, giving numerical coefficients  $_n\widehat{H}_{lm}$ .

The computation times given in Table 1 are averages over 5 random test-functions. Both for the direct and inverse spin  $\pm 2$  transforms, they range between  $1.0 \times 10^{-1}$  seconds for  $L = 128$  and  $2.2 \times 10^1$  seconds for  $L = 1024$ . The equality of computation times for the positive and negative spins is an evident consequence of the similarity of the  $\pm 2$  cases in the expressions (28) and (30). The case  $n = 0$  corresponds to the scalar spherical harmonics transform, and is added for comparison. The related values range between  $2.7 \times 10^{-2}$  seconds for  $L = 128$  and 6.5 seconds for  $L = 1024$ . To summarize, computation times are of the order of seconds for a band limit  $L = 1024$ , in agreement with our previous intuitive estimations.

Spin	Time $L = 128$	Time $L = 256$	Time $L = 512$	Time $L = 1024$
	(sec)	(sec)	(sec)	(sec)
$n = 0$	$3.7e - 02$	$2.0e - 01$	$1.1e + 00$	$6.5e + 00$
	$2.7e - 02$	$1.4e - 01$	$8.1e - 01$	$6.2e + 00$
$n = 2$	$1.2e - 01$	$6.4e - 01$	$3.6e + 00$	$2.2e + 01$
	$1.0e - 01$	$5.0e - 01$	$2.9e + 00$	$2.1e + 01$
$n = -2$	$1.2e - 01$	$6.4e - 01$	$3.5e + 00$	$2.1e + 01$
	$1.0e - 01$	$5.0e - 01$	$2.9e + 00$	$2.1e + 01$

Table 1

Computation times for  $n = 0$  and  $n = \pm 2$  spherical harmonics transforms measured on a 2.20 GHz Intel Pentium Xeon CPU with 2 Gb of RAM memory. Times associated with the direct transforms are listed above the corresponding times for the inverse transform.

Both for the direct and inverse transforms, the evolution of the values reported as a function of the band limit also supports the  $\mathcal{O}(L^2 \log_2^2 L)$  behaviour of the related asymptotic complexity, as illustrated in figure 2 in comparison with an  $\mathcal{O}(L^3)$  slope. The ratio of computation times for the cases  $n = \pm 2$  and  $n = 0$  also reflects the simple fact that three scalar transforms are computed for each spin  $\pm 2$  transform.

In the present implementation based on the SpharmonicKit package, the required associated Legendre polynomials  $P_l^m(\cos \theta)$  are pre-calculated once for



all values of  $l$ ,  $\theta$ , and  $m$ , and stored in RAM memory. The pre-calculation computation time itself is of order  $\mathcal{O}(L^3)$  through the use of a recurrence relation in  $l$  on the associated Legendre polynomials. This pre-calculation is by definition not taken into account in the reported computation times, which consequently remain of order  $\mathcal{O}(L^2 \log_2^2 L)$ . The number of real values of associated Legendre polynomials  $P_l^m(\cos \theta)$  stored in RAM memory for all  $l$ ,  $\theta$ , and  $m$  is also of order  $\mathcal{O}(L^3)$ . The overall memory requirements allowing the direct and inverse transforms with the present numerical implementation correspondingly increase from 5.6 Mb for  $L = 128$ , to 32 Mb for  $L = 256$ , 220 Mb for  $L = 512$ , and 1.2 Gb for  $L = 1024$ . These memory requirements are easily accessible on a single standard computer.

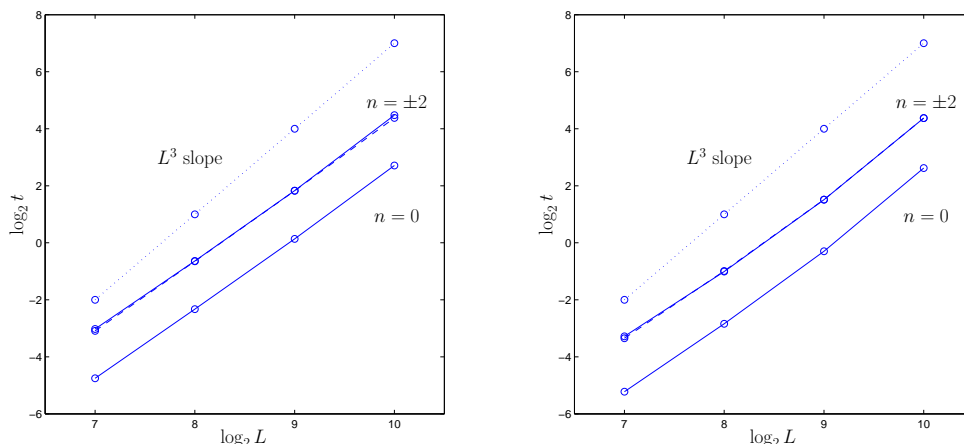


Figure 2. Evolution of computation times  $t$  displayed as  $\log_2 t - \log_2 L$  for the direct (left) and inverse (right) spin-weighted spherical harmonics transforms of spins  $n = 0$  (continuous line),  $n = +2$  (continuous line), and  $n = -2$  (dashed line). Computation times are measured in seconds on a 2.20 GHz Intel Pentium Xeon CPU with 2 Gb of RAM memory, and reported for the band limits  $L \in \{128, 256, 512, 1024\}$ . The  $\mathcal{O}(L^2 \log^2 L)$  asymptotic complexity is clearly illustrated when compared to an  $\mathcal{O}(L^3)$  slope (dotted line).

The absolute and relative numerical errors are defined as  $\max_{l,m} |{}_n \hat{G}_{lm} - {}_n \hat{H}_{lm}|$  and  $\max_{l,m} |({}_n \hat{G}_{lm} - {}_n \hat{H}_{lm}) / {}_n \hat{G}_{lm}|$  respectively, where  $|\cdot|$  here denotes the complex norm, and  $n \in \{0, \pm 2\}$ . The numerical errors associated with the  $\mathcal{O}(L^2 \log^2 L)$  spin-weighted spherical harmonics transforms given in Table 2 are averages for transforms over 5 random band-limited test-functions. Absolute and relative errors do not exceed the order of  $8.4 \times 10^{-9}$  and  $4.2 \times 10^{-7}$  respectively for band limits up to  $L = 1024$ .

Spin	Error $L = 128$	Error $L = 256$	Error $L = 512$	Error $L = 1024$
$n = 0$	$1.8\text{e} - 10$	$6.5\text{e} - 10$	$2.3\text{e} - 09$	$8.4\text{e} - 09$
	$9.7\text{e} - 10$	$5.7\text{e} - 09$	$1.6\text{e} - 08$	$1.1\text{e} - 07$
$n = 2$	$1.8\text{e} - 10$	$6.6\text{e} - 10$	$2.4\text{e} - 09$	$8.3\text{e} - 09$
	$7.2\text{e} - 10$	$4.2\text{e} - 09$	$4.6\text{e} - 08$	$4.2\text{e} - 07$
$n = -2$	$1.8\text{e} - 10$	$6.6\text{e} - 10$	$2.3\text{e} - 09$	$8.3\text{e} - 09$
	$9.8\text{e} - 10$	$2.9\text{e} - 09$	$3.1\text{e} - 08$	$1.2\text{e} - 07$

Table 2

Errors are measured on a 2.20 GHz Intel Pentium Xeon CPU with 2 Gb of RAM memory. Absolute errors after inverse and direct transforms are listed above the corresponding relative errors.

The  $\mathcal{O}(L^2 \log_2^2 L)$  implementation of the spin  $\pm 2$  spherical harmonics transforms is therefore stable for band limits up to  $L = 1024$ . The numerical stability of the algorithm might also have been inferred from the corresponding stability of the Driscoll and Healy fast direct scalar spherical harmonics transform algorithm, tested for band limits up to  $L = 1024$  [25,26]. The only potential source of instability is related to the multiplication factor  $\cot^p \theta / \sin^q \theta$  defining the scalar functions associated with a spin  $\pm 2$  function in the calculation of a spin-weighted spherical harmonics transform from the relation (28). Each such factor indeed corresponds to a division by  $\sin^2 \theta$ , which induces multiplications by numbers of the order of  $L^2$  around the poles  $\theta = \{0, \pi\}$ , where  $L$  is the band limit considered. However such operations could only produce numerical instabilities for very high band limits, and obviously remain completely safe at  $L = 1024$ .

In conclusion, these results confirm that an exact and stable  $\mathcal{O}(L^2 \log_2^2 L)$  algorithm for the spin-weighted spherical harmonics transforms of band-limited spin  $\pm 2$  functions may be easily implemented on a  $2L \times 2L$  equi-angular grid in  $(\theta, \varphi)$  on the sphere. The theoretical exactness and the  $\mathcal{O}(L^2 \log_2^2 L)$  asymptotic complexity of our algorithm advantageously compare with the approximate  $\mathcal{O}(L^3)$  implementations produced by the separation of variables on pixelizations such as HEALPix and GLESP. Let us establish a brief comparison with the present HEALPix package<sup>2</sup>. First, a good numerical stability of the HEALPix package requires an iterative implementation. Second, at present, computation times for the analysis of megapixels maps are of the same order of magnitude (seconds) with our algorithm and the HEALPix implementation. But further numerical optimization of our preliminary code should allow

<sup>2</sup> See [healpix.jpl.nasa.gov](http://healpix.jpl.nasa.gov) for documentation and algorithm implementation (HEALPix2.1 software).

a better performance of our algorithm at such resolutions. Moreover, the better asymptotic complexity of our algorithm will evidently provide computation times lower than with the HEALPix package at higher resolutions. Notice that our algorithm requires larger but still easily accessible RAM memory.

## 4 Simulation of CMB polarization maps and computation of angular power spectra

In this last section, we first recall how a polarized electromagnetic radiation coming from one given direction may be described at each observation point in terms of the four Stokes parameters  $I$ ,  $Q$ ,  $U$ , and  $V$ , of a transverse rank 2 intensity tensor. Considering the distribution of the CMB signal on the sphere, we also study the transformation properties of these parameters under global and local transformations. Second, we introduce the scalar electric  $E$  and magnetic  $B$  linear polarization components whose scalar spherical harmonics coefficients participate to the definition of the invariant angular power spectra of the CMB temperature and polarization. We show that the scalar spherical harmonics coefficients of these  $E$  and  $B$  components are simple linear combinations of the spin  $\pm 2$  spherical harmonics coefficients of  $Q \pm iU$ . We finally illustrate the interest of the algorithm presented in § 3 for the efficient computation of the CMB invariant angular power spectra from the observable temperature  $T$  and linear polarization Stokes parameters  $Q$  and  $U$  (direct transform), or for the simulation of temperature and polarization maps from theoretical spectra (inverse transform).

Our discussion is based on the following CMB polarization introductory papers [4,5,6,7,8,9] and reviews [28,29,30,31].

### 4.1 Stokes parameters

The CMB is observed in each direction  $\omega = (\theta, \varphi)$  of the sky as an incoming radial radiation, to which is associated a transverse electromagnetic field thus lying in the tangent plane to the sphere at the point considered. In the tangent plane, we consider the basis  $(\hat{e}_\theta, \hat{e}_\varphi)$  attached to each point  $\omega$  on the unit sphere  $S^2$ , with  $\hat{e}_\theta$  pointing in the direction of increasing  $\theta$  along each meridian, and  $\hat{e}_\varphi$  in the direction of increasing  $\varphi$  along each parallel. In this so-called linear polarization basis  $(\hat{e}_\theta, \hat{e}_\varphi)$  at each point  $\omega$ , nearly monochromatic radiation around a frequency  $\omega_r$  may be decomposed as an electric field with components  $E_\theta(\omega_r, t) = \mathcal{R}e[\varepsilon_\theta(t)e^{-i\omega_r t}]$  and  $E_\varphi(\omega_r, t) = \mathcal{R}e[\varepsilon_\varphi(t)e^{-i\omega_r t}]$ . The complex amplitudes  $\varepsilon_\theta(t)$  and  $\varepsilon_\varphi(t)$  slowly vary in time relatively to the timescale set by the wave period. The intensity matrix  $\mathbf{I}$  associated with the

radiation in the tangent plane at the point considered simply reads as the time average of the electric field rank 2 tensor  $[\varepsilon_i^*(t)\varepsilon_j(t)]\hat{e}_i \otimes \hat{e}_j$ , for  $i, j \in \{\theta, \varphi\}$  [4,9]. It thus naturally decomposes on the  $2 \times 2$  matrix basis  $(\sigma_0, \sigma_1, \sigma_2, \sigma_3)$  formed by the identity matrix  $\sigma_0 = \mathbb{I}$ , and the Pauli matrices

$$\sigma_1 = \begin{bmatrix} 0 & 1 \\ 1 & 0 \end{bmatrix}, \quad \sigma_2 = \begin{bmatrix} 0 & -i \\ i & 0 \end{bmatrix}, \quad \sigma_3 = \begin{bmatrix} 1 & 0 \\ 0 & -1 \end{bmatrix}, \quad (33)$$

as

$$\mathbf{I} = \frac{1}{2} [I\sigma_0 + U\sigma_1 + V\sigma_2 + Q\sigma_3], \quad (34)$$

where the constants  $I$ ,  $U$ ,  $V$ , and  $Q$  define the four real Stokes parameters [32] associated with the radiation:

$$\begin{aligned} I &= \langle |\varepsilon_\theta(t)|^2 + |\varepsilon_\varphi(t)|^2 \rangle \\ Q &= \langle |\varepsilon_\theta(t)|^2 - |\varepsilon_\varphi(t)|^2 \rangle \\ U &= \langle \varepsilon_\theta^*(t)\varepsilon_\varphi(t) + \varepsilon_\theta(t)\varepsilon_\varphi^*(t) \rangle \\ V &= i\langle \varepsilon_\theta^*(t)\varepsilon_\varphi(t) - \varepsilon_\theta(t)\varepsilon_\varphi^*(t) \rangle. \end{aligned} \quad (35)$$

The brackets  $\langle \cdot \rangle$  denote statistical mean, estimated here through time averaging. If the two components  $\varepsilon_\theta(t)$  and  $\varepsilon_\varphi(t)$  are correlated, the radiation is said to be polarized. The positive parameter  $I$  may be identified with the overall intensity of radiation, while  $Q$  and  $U$  identify with the linear polarizations, and  $V$  with the circular polarization. Unpolarized radiation, or natural light, is therefore characterized by  $Q = U = V = 0$ .

As functions on the sphere,  $I(\omega)$ ,  $Q(\omega)$ ,  $U(\omega)$  and  $V(\omega)$  have different behaviours under both global inversion ( $\cdot''$ ) of the coordinates and local rotations ( $\cdot'$ ) of the basis vectors  $(\hat{e}_\theta, \hat{e}_\varphi)$  in the tangent plane at  $\omega = (\theta, \varphi)$ . A global inversion of the right-handed three-dimensional Cartesian coordinate system  $(o, o\hat{x}, o\hat{y}, o\hat{z})$  centered on the unit sphere induces the following modification of Cartesian coordinates:  $(x'', y'', z'') = (-x, -y, -z)$ . The spherical coordinates  $\omega = (\theta, \varphi)$  of a given point on  $S^2$  change according to  $\omega'' = (\theta'', \varphi'') = (\pi - \theta, \pi + \varphi)$ . Locally in the tangent plane, the global inversion also implies an inversion of the basis vector  $\hat{e}_\theta$ :  $(\hat{e}_\theta'', \hat{e}_\varphi'') = (-\hat{e}_\theta, \hat{e}_\varphi)$ . Consequently, the definitions (35) imply that  $I$  and  $Q$  have even parity,  $I''(\omega'') = I(\omega)$  and  $Q''(\omega'') = Q(\omega)$ , while  $U$  and  $V$  have odd parity,  $U''(\omega'') = -U(\omega)$  and  $V''(\omega'') = -V(\omega)$ . Under local rotations of the basis vectors  $(\hat{e}_\theta, \hat{e}_\varphi)$  by an angle  $\chi_0$ , the coordinates  $\vec{\varepsilon} = (\varepsilon_\theta, \varepsilon_\varphi)$  of vectors in the tangent plane at each considered point on the sphere transform through  $\vec{\varepsilon}' = r_{\chi_0} \cdot \vec{\varepsilon}$ , for the rotation matrix

$$r_{\chi_0} = \begin{bmatrix} \cos \chi_0 & \sin \chi_0 \\ -\sin \chi_0 & \cos \chi_0 \end{bmatrix}. \quad (36)$$

The corresponding transformation on the Stokes parameters may be directly given from their definition (35):  $I$  and  $V$  are invariant while  $Q$  and  $U$  are mixed by local rotations. Equivalently, one may also rewrite the intensity matrix as

$$\mathbf{I} = \frac{1}{2} [I\sigma_0 + V\sigma_2 + (Q + iU)\sigma_+ + (Q - iU)\sigma_-], \quad (37)$$

with  $\sigma_{\pm} = (\sigma_3 \mp i\sigma_1)/2$ . Under local rotations, the Pauli matrices transform as  $\sigma'_{\mu} = r_{\chi_0} \cdot \sigma_{\mu} \cdot r_{\chi_0}^T$ , for  $\mu = \{0, 1, 2, 3\}$ . The matrices  $\sigma_0$  and  $\sigma_2$  are thus invariant, while  $\sigma_{\pm}$  transform as  $\sigma'_{\pm} = e^{\mp 2i\chi_0} \sigma_{\pm}$ . Consequently the four Stokes parameters are associated with spin functions on the sphere. The intensity  $I(\omega)$  and the circular polarization parameter  $V(\omega)$  are scalar functions. The combinations  $(Q \pm iU)(\omega)$  are spin  $\pm 2$  functions:  $(Q \pm iU)'(\omega) = e^{\mp 2i\chi_0} (Q \pm iU)(\omega)$ . Notice that under parity these two combinations transform in one another:  $(Q \pm iU)''(\omega'') = (Q \mp iU)(\omega)$  [5,9].

#### 4.2 Computation of power spectra and maps simulation

It is assumed that the physics of the CMB is invariant under global inversion of the coordinates and under local rotations (cosmological principle). It is therefore suitable to relate the observables  $I$ ,  $Q$ ,  $U$ , and  $V$  to invariant physical quantities. The intensity  $I(\omega)$  defines the CMB temperature anisotropies  $T(\omega)$  and is indeed itself invariant under the transformations considered. The polarization of the CMB is essentially induced through Thomson scattering of originally unpolarized radiation, near the surface of last scattering. As no circular polarization may arise from Thomson scattering, the CMB polarization is completely described in terms of the two linear polarization Stokes parameters  $Q$  and  $U$ . It is equivalently defined by their spin  $\pm 2$  combinations  $Q \pm iU$ . Associated polarization components, real scalar functions on the sphere and parity eigenmodes, are naturally defined from  $Q \pm iU$  in terms of the raising  $\bar{\partial}$  and lowering  $\partial$  operators respectively given in (19) and (20). These components

$$\tilde{E}(\omega) = -\frac{1}{2} [\bar{\partial}^2 (Q + iU)(\omega) + \partial^2 (Q - iU)(\omega)], \quad (38)$$

and

$$\tilde{B}(\omega) = \frac{i}{2} [\bar{\partial}^2 (Q + iU)(\omega) - \partial^2 (Q - iU)(\omega)], \quad (39)$$

have even and odd parities and are therefore referred to as electric and magnetic components respectively [5]. Let us consider the decomposition of the spin  $\pm 2$  functions  $Q \pm iU$  in spin-weighted spherical harmonics and the relations  ${}_2Y_{lm} = N_{(l2)} \bar{\partial}^2 Y_{lm}$  and  ${}_{-2}Y_{lm} = N_{(l2)} \partial^2 Y_{lm}$ , with  $N_{(l2)} = [(l-2)!/(l+2)!]^{1/2}$ , induced from (24) and (25). The application of the raising and lowering operators on this decomposition through the relations (21) to (23) gives

$\hat{\tilde{E}}_{lm} = \hat{E}_{lm}/N_{(l2)}$  and  $\hat{\tilde{B}}_{lm} = \hat{B}_{lm}/N_{(l2)}$ , where

$$\hat{E}_{lm} = -\frac{1}{2} \left( {}_{+2}(\widehat{Q + iU})_{lm} + {}_{-2}(\widehat{Q - iU})_{lm} \right), \quad (40)$$

and

$$\hat{B}_{lm} = \frac{i}{2} \left( {}_{+2}(\widehat{Q + iU})_{lm} - {}_{-2}(\widehat{Q - iU})_{lm} \right), \quad (41)$$

define the properly normalized real  $E(\omega)$  and  $B(\omega)$  components. The transformation properties of these coefficients under local rotations and parity directly follow from the corresponding transformations for  $\hat{E}(\omega)$ ,  $\hat{B}(\omega)$ , and those of the scalar spherical harmonics. They are explicitly invariant under local rotations, while under parity,  $\hat{E}''_{lm} = (-1)^l \hat{E}_{lm}$  and  $\hat{B}''_{lm} = (-1)^{l+1} \hat{B}_{lm}$  [9].

The statistics of a Gaussian (in first approximation) and stationary (cosmological principle) CMB is completely characterized in terms of its temperature and polarization two-points correlation functions. The corresponding invariant angular power spectra are naturally those associated with the temperature  $TT$ , the polarizations  $EE$  and  $BB$ , and the cross-correlation between the temperature and electric polarization component  $TE$ :

$$\begin{aligned} \langle \hat{T}_{l'm'}^* \hat{T}_{lm} \rangle &= C_l^{TT} \delta_{ll'} \delta_{mm'} \\ \langle \hat{E}_{l'm'}^* \hat{E}_{lm} \rangle &= C_l^{EE} \delta_{ll'} \delta_{mm'} \\ \langle \hat{B}_{l'm'}^* \hat{B}_{lm} \rangle &= C_l^{BB} \delta_{ll'} \delta_{mm'} \\ \langle \hat{T}_{l'm'}^* \hat{E}_{lm} \rangle &= C_l^{TE} \delta_{ll'} \delta_{mm'}. \end{aligned} \quad (42)$$

These physical quantities are indeed invariant under local rotations and parity. The  $TB$  and  $EB$  cross-correlations are specifically excluded from the requirement of invariance under parity.

The  $E$  and  $B$  components of polarization not only define invariant physical angular power spectra, but they are also associated with different mechanisms of production of the radiation, corresponding to different theoretical cosmological models. Scalar primordial energy density perturbations only produce the  $E$  polarization component, while vector and tensor (*i.e.* gravity waves) perturbations produce both  $E$  and  $B$  polarization components. The decoupling of the CMB polarization analysis into its  $E$  and  $B$  components, thus also allows to study its scalar, vector, or tensor origins, and in particular to probe the existence of primordial gravity waves [5,6,7,8,9].

On the one hand, from the theoretical point of view, the temperature and polarization angular power spectra in (42) may be computed from the corresponding  $T$ ,  $E$ , and  $B$  components, which are directly accessible for a given cosmological model. From the observational point of view, the scalar ( $\hat{T}_{lm}$ ) and spin  $\pm 2$  ( ${}_{\pm 2}(\widehat{Q \pm iU})_{lm}$ ) direct spherical harmonics transforms are required in

relations (40), (41), and (42) for the estimation of the  $TT$ ,  $EE$ ,  $BB$ , and  $TE$  power spectra [5]. On the other hand, the simulation of  $T$ ,  $Q$ , and  $U$  maps from given theoretical angular power spectra requires the corresponding inverse transforms. The algorithm developed in § 3 proposes an exact computation of the scalar and spin  $\pm 2$  spherical harmonics transforms up to the band limit  $L$  on  $2L \times 2L$  equi-angular grids on the sphere, with an  $\mathcal{O}(L^2 \log_2^2 L)$  asymptotic complexity.

### 4.3 Numerical illustration

We finally apply our algorithm to simulate CMB maps and angular power spectra, for illustration of its precision and speed. In that perspective we start from the temperature and polarization spectra  $C_l^{TT}$ ,  $C_l^{EE}$ , and  $C_l^{TE}$  defined by the present concordance cosmological model [2] (the  $BB$  polarization spectrum is identically null:  $C_l^{BB} = 0$ ). These spectra are represented in figure 4 up to a band limit  $L = 1024$ . First, spherical harmonics coefficients  $\hat{T}_{lm}$  and  $\hat{E}_{lm}$  are built up as the two marginal complex Gaussian realizations arising from a jointly Gaussian statistical distribution with variances  $C_l^{TT}$  and  $C_l^{EE}$ , and a covariance  $C_l^{TE}$ . Second, we produce the  $T$ ,  $Q$ , and  $U$  maps by inverse scalar and spin  $\pm 2$  transforms, through the relations (40) and (41), with  $\hat{B}_{lm} = 0$ . These maps are given in figure 3 on a  $2L \times 2L$  equi-angular pixelization on the sphere.

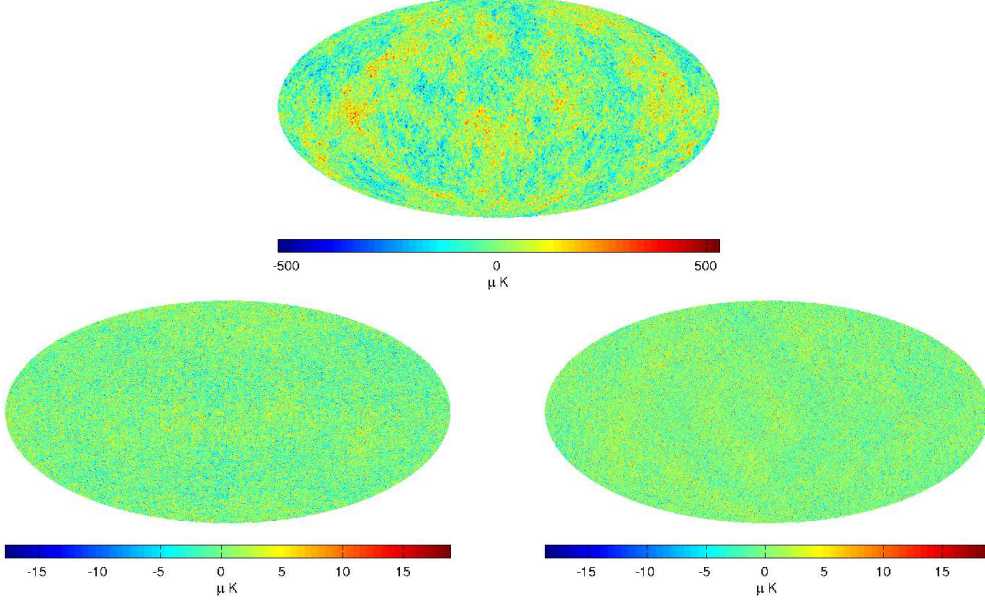


Figure 3. Mollweide projection of the  $T$  (top),  $Q$  (bottom left), and  $U$  (bottom right) simulated Gaussian CMB maps computed from the power spectra  $C_l^{TT}$ ,  $C_l^{EE}$ ,  $C_l^{BB} = 0$ , and  $C_l^{TE}$  defined by the present concordance cosmological model up to the band limit  $L = 1024$ . The exact  $\mathcal{O}(L^2 \log^2 L)$  scalar and spin  $\pm 2$  inverse spherical harmonics transforms on  $2L \times 2L$  equi-angular grids on the sphere is applied.

We then recompute spherical harmonics coefficients  $\hat{T}'_{lm}$ ,  $\hat{E}'_{lm}$ , and  $\hat{B}'_{lm}$  by direct scalar and spin  $\pm 2$  transforms of the maps. Within the numerical accuracy of the computer, the  $B$  polarization coefficients are identically null, in perfect agreement with the original data:  $\hat{B}'_{lm} = 0$ . We finally estimate the temperature and polarization angular power spectra from those coefficients as:

$$\begin{aligned}
C_l^{TT'} &= \frac{1}{2l+1} \sum_{m=-l}^l |\hat{T}'_{lm}|^2 \\
C_l^{EE'} &= \frac{1}{2l+1} \sum_{m=-l}^l |\hat{E}'_{lm}|^2 \\
C_l^{TE'} &= \frac{1}{2l+1} \sum_{m=-l}^l \hat{T}'_{lm}^* \hat{E}'_{lm},
\end{aligned} \tag{43}$$

and  $C_l^{BB'} = \sum_{m=-l}^l |\hat{B}'_{lm}|^2 / (2l+1) = 0$ . These estimators follow chi-square distributions with  $2l+1$  degrees of freedom. For  $X \in \{TT, EE, BB, TE\}$ , this induces a fractional uncertainty  $\sigma_{C_l^{X'}} / C_l^X = [2/(2l+1)]^{1/2}$  in the estimation. This cosmic variance is large at low  $l$  and small at high  $l$ . The figure 4 represents the good coincidence between the original and estimated spectra up to the corresponding uncertainty at each  $l$ .



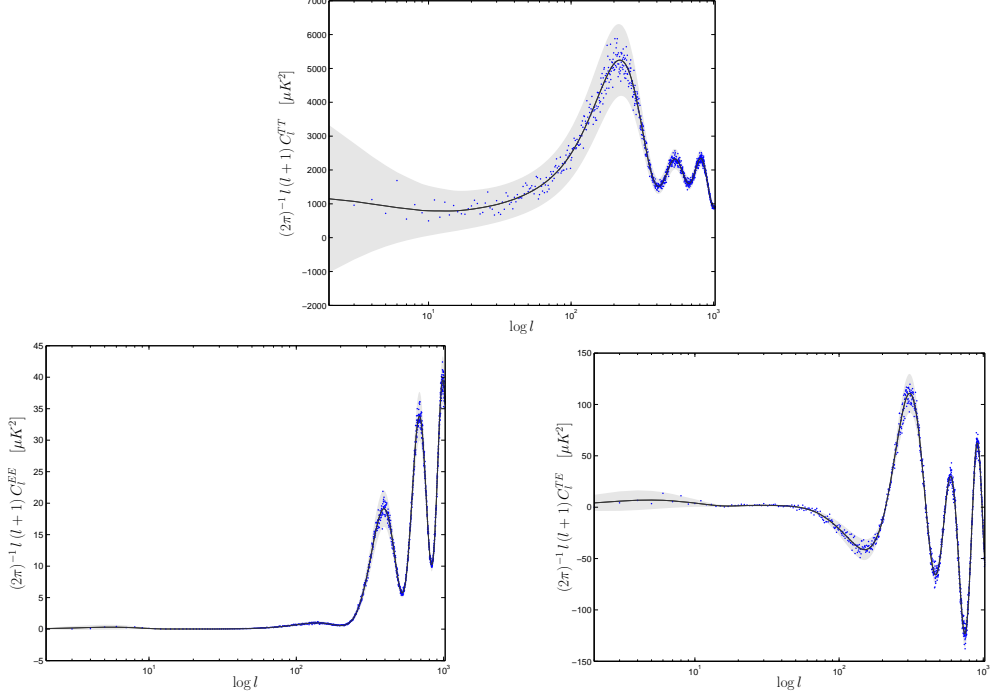


Figure 4. CMB temperature and polarization angular power spectra  $C_l^{TT}$  (top),  $C_l^{EE}$  (bottom left), and  $C_l^{TE}$  (bottom right) of the present concordance cosmological model, up to a band limit  $L = 1024$  and in  $\mu K^2$ . Direct transforms through the exact  $\mathcal{O}(L^2 \log^2 L)$  scalar and spin  $\pm 2$  spherical harmonics transforms on  $2L \times 2L$  equi-angular grids on the sphere are performed to produce the estimated spectra from the simulated Gaussian CMB maps for  $T$ ,  $Q$ , and  $U$ . The original (continuous lines) and estimated (scattered points) spectra coincide within the  $3\sigma$  uncertainty defined by the cosmic variance (grey region).

The computation time associated with the overall procedure is 150 seconds on a 2.20 GHz Intel Pentium Xeon CPU with 2 Gb of RAM memory. In summary, this application illustrates the good precision and speed performances of our fast and exact algorithms, coherently with the results reported in tables 1 and 2.

## 5 Conclusion

In conclusion, we developed an exact fast, and stable algorithm for the spin  $\pm 2$  spherical harmonics transforms of band-limited functions with band limit  $L$  on  $2L \times 2L$  equi-angular pixelizations in  $(\theta, \varphi)$  on the sphere. The algorithm is based the Driscoll and Healy fast scalar spherical harmonics transform algorithm. The exactness of the computation on equi-angular grids relies on a sampling theorem on the sphere. The associated asymptotic complexity is of

order  $\mathcal{O}(L^2 \log_2^2 L)$ , to be compared with an *a priori*  $\mathcal{O}(L^4)$  asymptotic complexity. The numerical stability is a consequence of the corresponding stability for the Driscoll and Healy fast scalar transform. The numerical implementations produced confirm the characteristics of the algorithm.

This algorithm can be applied in the spectral analysis of arbitrary spin  $\pm 2$  signals on the sphere, components of transverse, symmetric, and traceless rank 2 tensor fields under local rotations.

We considered in detail the particular application of the CMB polarization analysis, which is of major interest for future CMB experiments. The statistics of a Gaussian and stationary CMB signal is completely characterized by its temperature ( $TT$ ), polarization ( $EE$  and  $BB$ ), and cross-correlation ( $TE$ ) angular power spectra. The precise estimation of these spectra from the corresponding observable Stokes parameters  $T$ ,  $Q$ , and  $U$  requires the calculation of the direct scalar and spin  $\pm 2$  spherical harmonics transforms of the temperature  $T$  and of the combinations  $Q \pm iU$ , respectively. The simulations of temperature and polarization maps from theoretical power spectra requires the corresponding inverse transforms. In this context, the computation times for the analysis of megapixels CMB maps such as those from the ongoing WMAP experiment or the forthcoming Planck experiment, are reduced to seconds on a single standard computer. Our algorithm on equi-angular grids represents an alternative to existing algorithms on the widely used HEALPix and GLESP pixelizations, which achieve comparable computation times on megapixels maps. However, the theoretical exactness and  $\mathcal{O}(L^2 \log_2^2 L)$  asymptotic complexity of our algorithm advantageously compare with the approximate  $\mathcal{O}(L^3)$  HEALPix and GLESP implementations.

## Acknowledgements

The authors wish to thank P. Vielva, J.-P. Antoine, B. Barreiro, and E. Martínez-González for valuable comments and discussions. Y. W. acknowledges support of the Swiss National Science Foundation (SNF) under contract No. 200021-107478/1. He is also postdoctoral researcher of the Belgian National Science Foundation (FNRS).

## References

- [1] L. Page *et al.*, *Astrophys. J. Suppl.* **148**, 233 (2003).
- [2] D. N. Spergel *et al.*, *Astrophys. J. Suppl.* **148**, 175 (2003).

- [3] F. R. Bouchet, preprint astro-ph/0401108 (2004).
- [4] A. Kosowsky, Ann. Phys. **246**, 49 (1996).
- [5] M. Zaldarriaga and U. Seljak, Phys. Rev. D **55**, 1830 (1997).
- [6] U. Seljak and M. Zaldarriaga, Phys. Rev. Lett. **78**, 2054 (1997).
- [7] M. Kamionkowski, A. Kosowsky, and A. Stebbins, Phys. Rev. Lett. **78**, 2058 (1997).
- [8] M. Kamionkowski, A. Kosowsky, and A. Stebbins, Phys. Rev. D **55**, 7368 (1997).
- [9] W. Hu and M. White, Phys. Rev. D **56**, 596 (1997).
- [10] K. M. Górski, E. Hivon, A. J. Banday, B. D. Wandelt, F. K. Hansen, M. Reinecke, and M. Bartelman, Astrophys. J. **622**, 759 (2005).
- [11] B. F. Roukema and B. Lew, preprint astro-ph/0409533 (2004).
- [12] A. G. Doroshkevich, P. D. Naselsky, O. V. Verkhodanov, D. I. Novikov, V. I. Turchaninov, I. D. Novikov, P. R. Christensen, and L.-Y. Chiang, Int. J. Mod. Phys. D **14**, 275 (2005).
- [13] A. G. Doroshkevich, P. D. Naselsky, O. V. Verkhodanov, D. I. Novikov, V. I. Turchaninov, I. D. Novikov, P. R. Christensen, and L.-Y. Chiang, preprint astro-ph/0501494 (2005).
- [14] D. A. Varshalovich, A. N. Moskalev, and V. K. Khersonskii, *Quantum Theory of Angular Momentum*, First Edition Reprint, World Scientific, Singapore (1989).
- [15] M. Abramowitz and I. Stegun, *Handbook of mathematical functions*, Dover Publications Inc., New York (1965).
- [16] D. M. Brink and G. R. Satchler, *Angular Momentum*, Third Edition, Clarendon Press, Oxford (1993).
- [17] E. T. Newman and R. Penrose, J. Math. Phys. **7**, 863 (1966).
- [18] J. N. Goldberg, A. J. Macfarlane, E. T. Newman, F. Rohrlich, and E. C. G. Sudarshan, J. Math. Phys. **8**, 2155 (1967).
- [19] M. Carmeli, J. Math. Phys. **10**, 569 (1969).
- [20] J. R. Driscoll and D. M. Healy Jr., Adv. in Appl. Math. **15**, 202 (1994).
- [21] D. K. Maslen and D. N. Rockmore, in Proc. DIMACS Workshop on Groups and Computation 28, ed. L. Finkelstein and W. Kantor, American Math. Soc., Providence, 183 (1997).
- [22] P. J. Kostelec and D. N. Rockmore, technical report SFI-03-11-060 (2003).
- [23] D. K. Maslen and D. N. Rockmore, J. American Math. Soc. **10**, 169 (1997).
- [24] Y. Wiaux, L. Jacques, P. Vielva, and P. Vanderghenst, preprint astro-ph/0508516, Astrophys. J. in press (2005).

- [25] D. M. Healy Jr., D. N. Rockmore, P. J. Kostelec, and S. Moore, J. Fourier Anal. and Applic. **9**, 341 (2003).
- [26] D. M. Healy Jr., P. J. Kostelec, and D. N. Rockmore, Adv. in Comput. Math. **21**, 59 (2004).
- [27] P. J. Kostelec, D. K. Maslen, D. N. Rockmore, and D. M. Healy Jr., J. Comput. Phys. **162**, 514 (2000).
- [28] W. Hu and M. White, New A **2**, 323 (1997).
- [29] A. Kosowsky, New A Rev. **43**, 157 (1999).
- [30] P. Cabella and M. Kamionkowski, preprint astro-ph/0403392 (2004).
- [31] Y.-T. Lin and B. D. Wandelt, preprint astro-ph/0409734 (2004).
- [32] J. D. Jackson, *Classical Electromagnetism*, Second Edition, J. Wiley & Sons Inc., New York (1975).